CONF-780952--16

MASTER

SUPERCONDUCTING SPIN TIPPING SOLENOIDS FOR ZGS POLARIZED BEAM FACILITY

by

S-T Wang, K. Mataya, A. Paugys, and C. J. Chen

Prepared for

1978 Applied Superconductivity Conference

Pittsburgh, PA

September 28, 1978

NOTICE

This report was prepared as an account of work sponsored by the United States Government. Neither the United States nor the United States Department of Energy, nor any of their employees, nor any of their contractors, subcontractors, or their employees, makes any warranty, express or implied, or assumes any legal liability or responsibility for the accuracy, completeness or usefulness of any information, apparatus, product or process disclosed, or represents that its use would not infringe privately owned rights.

U of C-AUA-USDOE

ARGONNE NATIONAL LABORATORY, ARGONNE, ILLINOIS

Operated under Contract W-31-109-Eng-38 for the

U. S. DEPARTMENT OF ENERGY

DISTRIBUTION OF THIS DOCUMENT IS UNLIMITED

SUPERCONDUCTING SPIN TIPPING SOLENOIDS FOR ZGS POLARIZED BEAM FACILITY*

S-T. Wang, K. Mataya, A. Paugys, and C. J. Chen

ABSTRACT

Two superconducting solenoids have been designed and built for the Argonne Zero Gradient Synchrotron (ZGS) Polarized Proton Beam Facility. Each solenoid will have a central field of 8.0 T, an effective field length of about 1.75 m, and a cold clear bore of 11.5 cm. It will generate a spin-tipping integral field of about 14 T-m. The integral field homogeneity over the cold bore is ± 4%. The magnet stored energy is about 0.7 MJ.

Described in detail is the stability simulation on a high current density intrinsic stable coil. Comparisons are made between the simulation data and data obtained from the magnet performance tests. The cryostat design and construction are also presented.

I. INTRODUCTION

The polarized beam at the ZGS is normally polarized up or down. However, many experiments require the polarization rotable around the beam direction so that it can be horizontal and at right angles to the beam. The two solenoids are designed to accomplish a total rotation of 90° for the ZGS 12 GeV polarized proton beam.

II. MAGNET DESIGN ASPECTS

As shown in Fig. 1, the magnet coil is a 1.8 m long solenoid with coil I.D. 12.14 cm and coil O.D. 20.93 cm. The detailed magnet parameters are given in Table I.

Two kinds of conductors are available for the first solenoid. The conductor short sample specifications and their relative locations within the coil winding are indicated in Table I. The bore conductor of either kind is a rectangular composite of NbTi and Cu of dimentions 2.89 mm x 1.45 mm. The NbTi filament diameter is 88 μ for both conductors. However, conductor A has 180 filaments, a ratio of Cu to NbTi equal to 1.8:1, and a short sample characteristic of 1125 A at 7.5 T. On the other hand, conductor B has 132 filaments, Cu to NbTi ratio equal to 2.6:1, and a short sample characteristic of 900 A at 7.5 T. The twist pitch of both conductors is 1 twist per 2.54 cm. One typical result of short sample tests for both conductors A and B is shown in Fig. 2. It was a great surprise to find that severe "training" effects existed for both conductors. Furthermore, different samples train in different manners despite the fact that the sample was firmly supported in a sample holder. The causes for the short sample training are not clear. One of the probable causes is that poor metallurgical bonding exists between the NbTi filament and the copper stabilizer in the composite. This problem presents a serious difficulty in the designing of the solenoid.

Stability simulations were investigated using a 6 layer small solenoid which was noninductively wound in a Micarta coil form. The conductor in the solenoid is thermally insulated from the liquid helium. A heater was wrapped to the middle turn in the innermost layer. The heater is pulsed and an on-time of about 10 ms is chosen for most of the simulation experiments. The minimum propagating current was measured as a function of the heater perturbing energy. A total of four simulation coils were wound. Two were wound with conductor A. The other two were wound with conductor B.

Manuscript received September 28, 1978.
*Work supported by the U. S. Department of Energy.

For each conductor, one of the two coils was wound without epoxy and the other was wett wound with fiberglass epoxy between layers. The epoxy is Stycast 2850 Ft. The results of these simulation tests are shown in Fig. 3. It is seen that, in general, the potted coil performs slightly better than the non-potted coil. Furthermore, despite the fact that conductor A has more superconductor than conductor B, conductor B performs better than conductor A. Based on these investigations, it was decided to place conductor B in the high field region, to choose a design current of 700 A at 8 T, and to wind the solenoid without epoxy.

The coil structure is as shown in Fig. 1. The electrical insulation of the conductor is 0.063 mm thick Formvar coating. Therefore, there is little thermal conduction from turn to turn. Between layers, 0.025 mm Mylar was used for additional interlayer insulation. Hence, interlayer cooling is negligibly small. There is no provision for liquid helium circulation throughout the coil winding. However, both end turns of each layer are in direct contact with liquid helium. Any heat generation can only be removed along the whole length of conductor in each layer. For this reason, conductor splices were made at either the first turn or the last turn of a given layer. Because of the poor cooling design, one has to make sure that there is no short anywhere inside the winding. The poorly-cooled coil has an important advantage. That is, the velocity of propagation of the normal zone is so large that in a few seconds the entire coil becomes normal, ensuring an even dissipation of magnet stored energy over the entire length of conductor. Therefore, the magnet may have unlimited quenches without any external protection.

Two layers of stainless steel outer-banding are wound to reduce the hoop load of the superconducting composite. The stainless steel is tensioned to half of its yield stress and it is electrically insulated from both the winding and the end flanges of the bore tube.

It is desirable that the fringing fields along the solenoid ends decrease sharply. To accomplish this, two iron discs of 7.5 cm thick each are attached to the coil end flanges.

III. CRYOSTAT DESIGN ASPECTS

The cross section of the cryostat is shown in Fig. 4. The cold mass is supported at each end by three epoxy fiberglass tension members. The tension members are oriented at an angle so that there is no stress developed as the cold mass is cooled down to 4.2 K.

The nitrogen shield is made of stainless steel to reduce eddy current and the associated electromagnetic force should the magnet quench. It is cooled by four parallel liquid nitrogen copper lines spaced evenly over the shield surface. It is suspended by fiberglass support link similar in design to that of cold mass support system.

The magnet will be precooled by liquid nitrogen. The liquid nitrogen will be flushed out, then the magnet will be precooled further by liquid helium. A precooling line is used to introduce the liquid/gas helium evenly along the solenoid. A liquid-nitrogen extraction line runs down from the neck of the cryostat tower to the lowest spot in the helium vessel. Both lines terminate at the neck of the cryostat tower so that thermal oscillations will not be generated in these lines.

The helium vessel is surrounded with 10 layers of insulation of aluminized Mylar while the nitrogen shield is wrapped with 50 layers of aluminized Mylar.

IV. FABRICATION OF MAGNET COILS AND CRYOSTAT

The coil fabrication is shown in Fig. 5. The conductor tension device is a dummy coil bobbin linked to an electrical clutch. The conductor, after passing through the tension bobbin, is guided by pulleys to the winding bore tube. The winding tension for the conductor is about 14 kg. The coil winding process was carefully controlled for the number of turns per layer; the packing uniformity and the winding dimensions. Fig. 6 illustrates the qualities of the winding as well as the cooling channels in the coil end region. Note that the end flanges are offset with respect to the bore tube so that the helium inventory below the magnet coil is minimized.

The coil assembly is shown in Fig. 7. A stainless steel bar welded to both end flanges is used as the supporting structure for the terminal conductors.

The cryostat assembly is shown in Fig. 8.

V. MAGNET PERFORMANCE

The coil assembly is tested in a vertical dewar. The magnet performance data is listed in Table II. The training characteristics are indicated in Fig. 2.

VI. ACKNOWLEDGEMENTS

The authors wish to express their deep appreciation to K. Wiggin of Argonne National Laboratory for his skillful work in the coil winding and the conductor splicing.

TABLE I
Magnet Design Parameters

Axial Winding Length (m)	1.8
Winding I.D. (cm)	12.14
Winding O.D. (cm)	20.93
Conductor, bare	1.45 mm x 2.895 mm
Insulation Formvar (mm)	0.063
Interlayer Mylar (mm)	0.0254
Number of Layers	27.0
Number of Turns per Layer	597.0
Total Number of Turns	16119.0
Design Current	708.0 A
Short Sample Current	1125.0 A at 7.5 T (A conductor) covers layer 8 to layer 27 900.0 A at 7.5 T (B conductor) covers layer 1 to layer 7
Peak Field	8.0 T
Central Field	8.0 T
Design Current Density	14470.0 A/cm^2
Inductance	2.85 H
Stored Energy	0.7 MJ
Total Conductor Length per Coil (m)	8374.0
Outer-Banding O.D. (cm)	21.6
Design Integral Field	14.0 T-m

TABLE II
Magnet Performance Data

Max. Current (A)	725.0
Max. Central Field (T)	8.2
Max. Peak Field (T)	8.2
Current Density in Conductor (A/cm^2)	17023.0
Average Current Density in Coil (A/cm^2)	14780.0
Stored Energy (MJ)	0.74
Max. Integral Field (T-m)	144.0

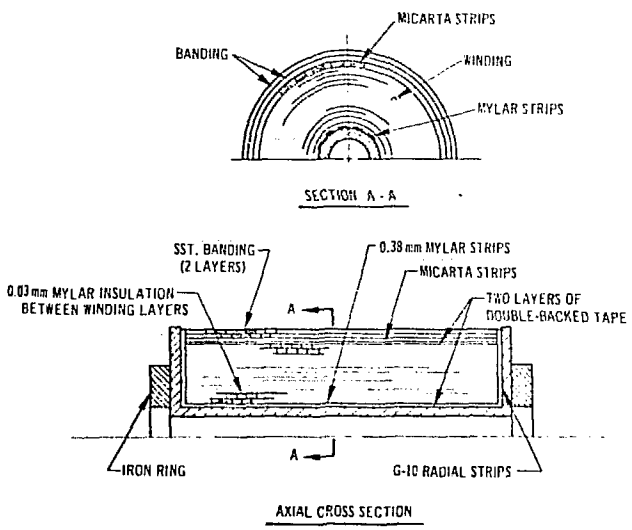

Fig. 1. Schematic Cross Section of the Magnet Coil

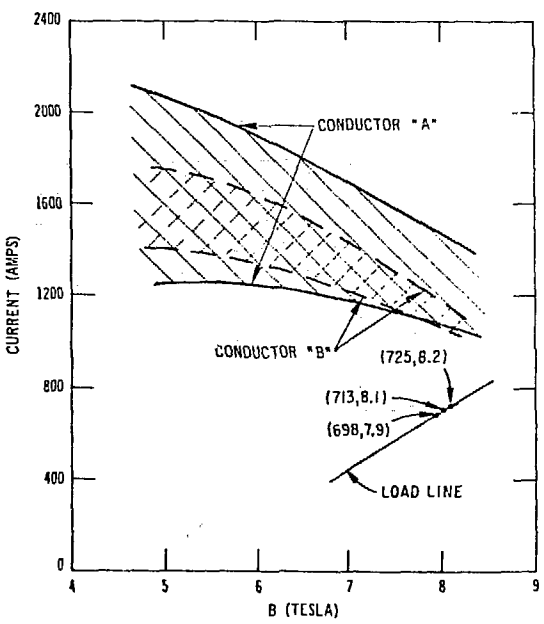

Fig. 2. Short Sample Test

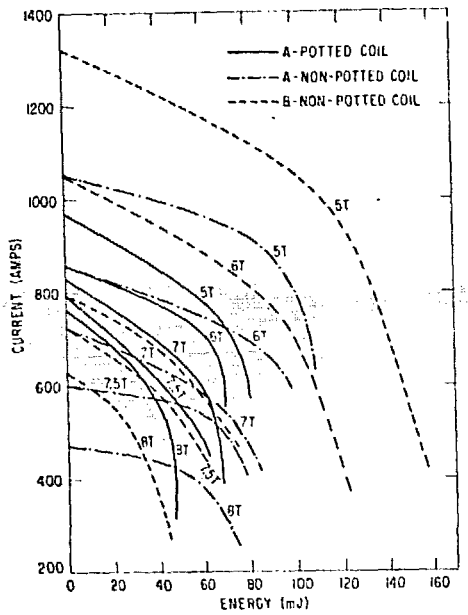

Fig. 3. Stability Simulation of Conductors

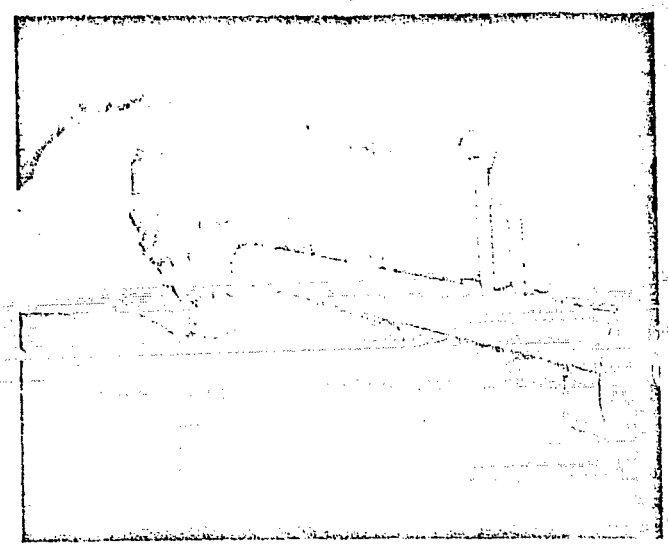

Fig. 5. Coil Fabrication

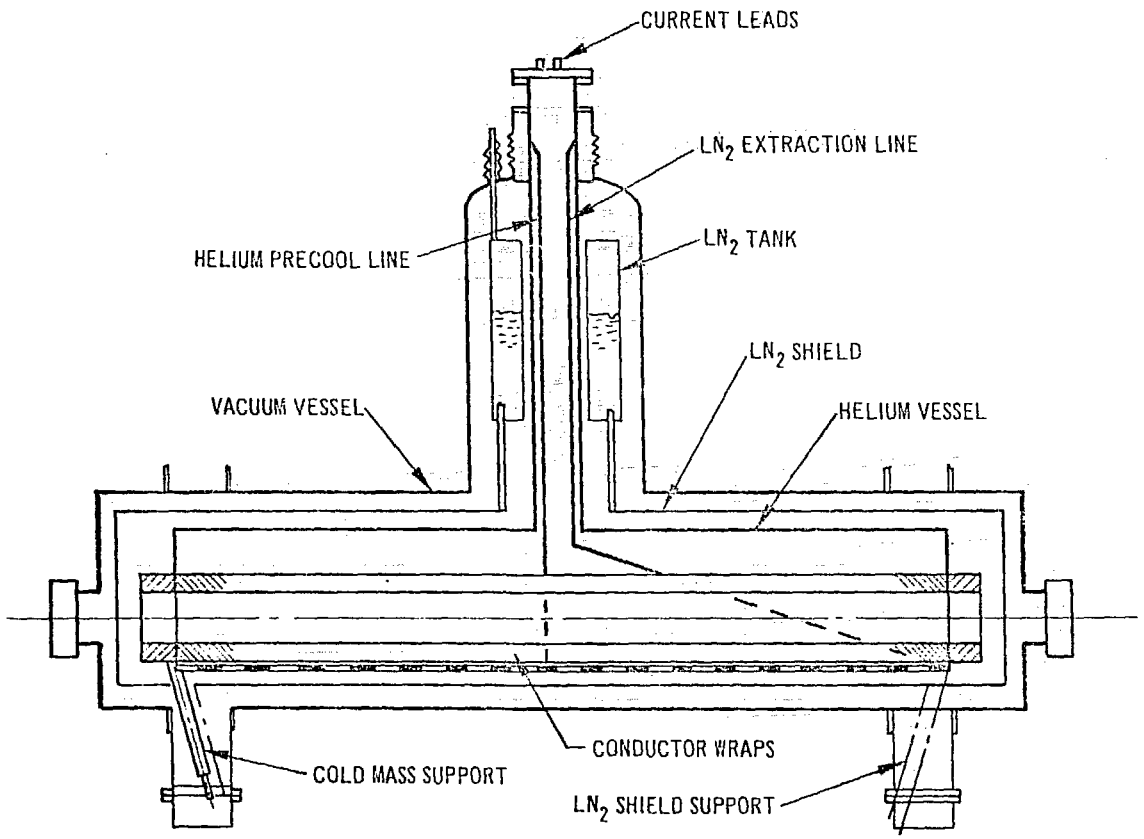

Fig. 4. Cryostat Cross Section

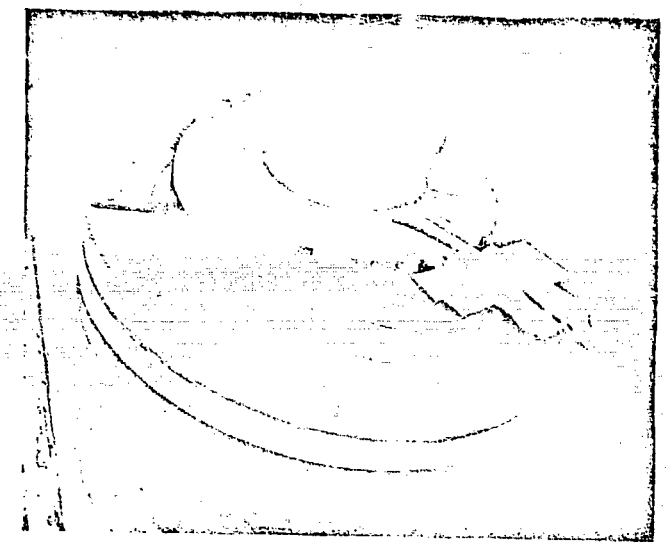

Fig. 6. Coil Winding Quality and the Cooling Channel in the Coil End Region

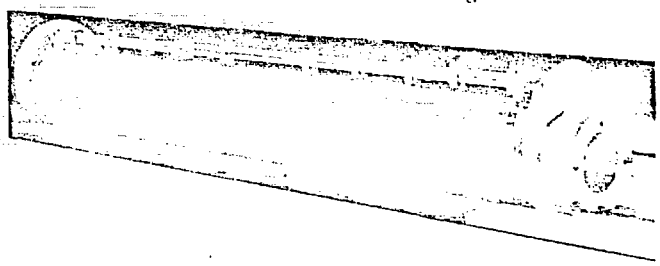

Fig. 7. Finished Coil Assembly

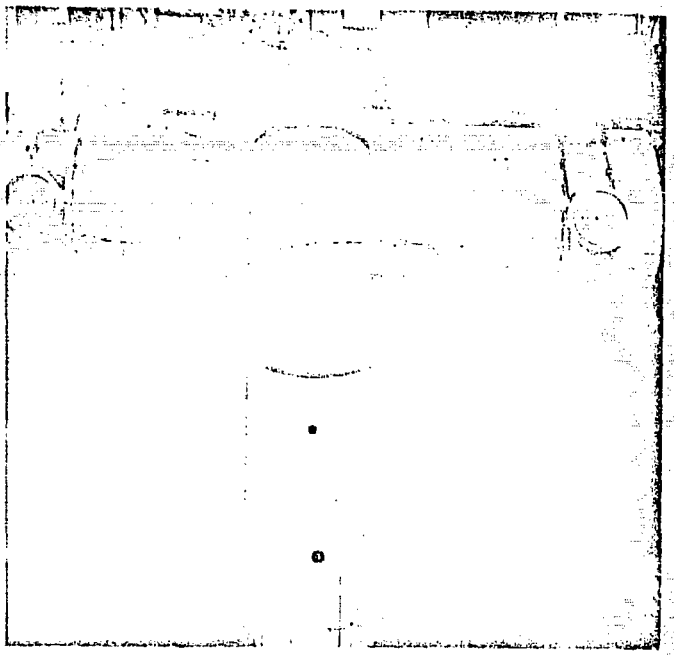

Fig. 8. Cryostat Assembly